Smart Structures and Systems, *Vol. 31*, *No. 1* (*2023*) *13-27*
https://doi.org/10.12989/sss.2023.31.1.013

Ultrasonic guided waves-based fatigue crack detection in a steel I-beam: an experimental study

Jiaqi Tu [1,3a], Xian Xu*[1], Chung Bang Yun [1b] and Yuanfeng Duan [2c]

[1] *College of Civil Engineering and Architecture*, *Key Laboratory of Space Structures of Zhejiang Province*, *Zhejiang University*, *866 Yuhangtang Road*, *Hangzhou*, *China*
[2] *College of Civil Engineering and Architecture*, *Institute of Transportation Engineering*, *Zhejiang University*, *866 Yuhangtang Road*, *Hangzhou*, *China*
[3] *WISDRI Engineering & Research Incorporation Limited*, *33 Xueyuan Road*, *Wuhan*, *China*

(*Received June 28*, *2022*, *Revised September 20*, *2022*, *Accepted September 21*, *2022*)

Abstract. Fatigue crack is a fatal problem for steel structures. Early detection and maintenance can help extend the service life and prevent hazards. This paper presents the ultrasonic guided waves-based (UGWs-based) fatigue crack detection of a steel I-beam. The semi-analytical finite element model has been built to obtain the wave propagation characteristics. Damage indices in both time and frequency domains were analyzed by considering the characteristic variations of UGWs including the amplitude, phase angle, and wave packet energy. The pulse-echo and pitch-catch methods were combined in the detection scheme. Lab-scale experiments were conducted on welded steel I-beams to verify the proposed method. Results show that the damage indices based on the characteristic variations in the time domain can identify and localize the fatigue crack before it enters the rapid growth stage. The damage severity can be reasonably evaluated by analyzing the time-domain damage indices. Two nonlinear damage indices in the frequency domain give earlier warnings of the fatigue crack than the time-domain damage indices do. The identification results based on the above two nonlinear indices are found to be less consistent under various excitation frequencies. More robust nonlinear techniques needed to be searched and tested for early crack detection in steel I-beams in further study.

Keywords: crack localization; damage indices; fatigue crack detection; steel beam; ultrasonic guided waves

1. Introduction

Fatigue damage has been a great concern for in-service steel structures. Early fatigue cracks often occur at the hot spots with high-stress concentration in steel components, due to initial material defects or intergranular pores after improper welding. Initial microcracks accumulate under cyclic loadings and become macroscopic after reaching about 80% of the structural fatigue life (Bathias and Pineau 2013, Rykaluk *et al*. 2018). The crack will eventually enter the unstable growing stage and may cause the failure of the structural component, or even lead to the sudden collapse of the entire structure. It has been reported that nearly 90% of the failure cases of metallic structures came from the fatigue problem (Santecchia *et al*. 2016). Therefore, regular inspections are necessary for the maintenance and management of steel structures (Farrar and Worden 2009, Guan *et al*. 2015, Raabe *et al*. 2019).

Various nondestructive testing (NDT) and structural health monitoring (SHM) technologies have been developed in the past decades, such as the eddy current method, X-ray, acoustic emission, and ultrasonic technique (Hoła and Schabowicz 2010, Rehman *et al*. 2016). Among these techniques, the ultrasonic guided waves (UGWs) method is an active NDT technique, which provides reliable structural health information based on the propagation characteristics of guided waves. Compared with the conventional vibration-based SHM techniques, the UGWs method is less vulnerable to low-frequency ambient vibrations and more sensitive to the local surface and subsurface defects. The sensing range and detection sensitivity can be improved simultaneously by optimizing the sensor excitation scheme and signal processing procedures. The UGWs method has been applied for the damage inspection of various types of structural members, including the composite plates (Garg *et al*. 2016), steel plates (Lim *et al*. 2017, Wang *et al*. 2018), pipes (Niu *et al*. 2018), cables (Schaal *et al*. 2016), steel bolts (Zhang *et al*. 2019), and steel rails (Wu *et al*. 2018, Wang *et al*. 2020). Mariani and Cawley (2021) proposed an automated damage detection framework based on the generalized likelihood ratio method and analyzed the UGW signals for long-range scanning of pipes under varying temperatures. Lim and Sohn (2020) input Lamb-wave signals into a convolutional neural network to measure the stress level of metallic plate-like structures under dynamic and static loadings. Yu *et al*. (2019) demonstrated the feasibility of using high-order-feature guided waves for detecting small defects in welded joints.

*Corresponding author, Ph.D., Professor,
E-mail: xianxu@zju.edu.cn
[a] Ph.D.
[b] Ph.D., Professor
[c] Ph.D., Professor

http://www.techno-press.org/?journal=sss&subpage=7
ISSN: 1738-1584 (Print), 1738-1991 (Online)

Generally, there are three stages of fatigue crack development for metallic members (Bathias and Pineau 2013, Molina and Chapetti 2018). In Stage I, the initial short crack grows along the shear stress plane dependent upon the loading direction. As the interfaces begin to slip around the crack tip region, the crack grows longer in the perpendicular direction, which is a typical feature in Stage II. Stage III means the rapid fracture and final failure of the steel member. At this stage, the stress in the crack tip region reaches the plastic strength and macroscopic cracks are observed. Steel I-beams are widely used as the major load-carrying members in industrial facilities. Due to inevitable initial defects and residual stress, fatigue cracks may develop easily in the weld zone and extend rapidly to other regions of the beam in the final stage of failure.

There are two kinds of methods for the quantitative analysis of guided wave signals on damage detection (Mitra and Gopalakrishnan 2016, Kundu 2019). The linear ultrasonic method analyzes the linear features of guided waves, which include the changes in amplitude, phase angle, and wave packet energy in the time domain. Linear methods have shown satisfying robustness for the identification and localization of macro-cracks (Olisa *et al*. 2021). Chua and Cawley (2020) investigated the performance of the fundamental shear horizontal wave mode at 85 kHz for the crack detection of a 6-in diameter pipe. Based on the baseline subtraction methodology, a 2-mm-long and 1-mm-deep notch at the outer surface was successfully detected.

The nonlinear ultrasonic method investigates the nonlinear features of UGWs in the frequency domain, which include the peak shift, the generation of sub-harmonics and high-order harmonic waves, the modulation between different frequencies, and the change of resonance frequencies. As for the harmonic phenomenon, when a group of sinusoidal guided waves propagates in a structural member, the interaction between the UGWs and microstructural defects generates a new group of second harmonic waves (SHWs) and higher orders of harmonic waves. By capturing and monitoring the variations of harmonic waves, it may be able to detect early-stage cracks, when their dimensions are in grain size order. Dutta *et al*. (2008) explored the possibility of harmonic waves-based crack detection on metallic structures and experimentally verified it. Lee *et al*. (2020) used the SHWs to identify the initiation of fatigue cracks in a T-shaped plate and quantify its growth based on a nonlinear index. The modulation phenomenon was also used to develop UGWs-based detection techniques, such as the frequency modulation method (Fierro and Meo 2015, Lim *et al*. 2017, Jeon *et al*. 2019) and sideband peak count (SPC) technique (Alnuaimi *et al*. 2020, Basu *et al*. 2021). Jeon *et al*. (2019) used the spectral correlation method to analyze the ultrasonic modulation components for crack detection of rotating steel shafts and sub-millimeter cracks were detected by using air-coupled transducers in pitch-catch mode. Basu *et al*. (2021) used the SPC technique on the early-stage damage identification of reinforced concrete structures.

The goal of this research is to detect the fatigue crack in a welded I-beam before it enters the rapid failure stage, i.e., Stage III. To the authors' knowledge, there are few studies on the UGWs-based fatigue crack detection of welded I-beams. There are several issues with the feasibility and sensitivity of the UGWs method for practical implementations. The main challenges include the control of the dispersion effect for the wave propagation in the I-beam, the interpretation of UGW signals, and the signal processing for the detection of crack existence and location. To tackle the challenges above, the excitation strategy shall be carefully selected to reduce the dispersion effect. Reliable damage indices shall be built for the analysis of the UGW signal. And experiments shall be carried out to observe the wave propagation characteristics and investigate their variations with crack development.

The paper is organized as follows. Section 2 describes the selection of the crack detection scheme. Experimental details are given in Section 3. Crack detection results are presented in Section 4. The factor analysis of different excitation strategies is carried out in Section 5. Finally, the conclusions of this study are summarized in Section 6.

2. Detection method of fatigue crack

In this research, the crack detection schemes mainly include two parts: the excitation strategy and the signal processing procedure, to achieve the crack identification and localization.

2.1 Excitation strategy

The propagation of UGWs is easily distorted by the geometrical or material changes in the waveguide. Therefore, it is very sensitive to the perturbations occurring on the waveguide, such as the crack and delamination. For a structural member with a complex configuration, the dispersion characteristics and multi-scattering waves affect the sensitivity and accuracy of the UGWs-based crack detection. Learning the propagation features of UGWs is the first step toward the effective adoption of this technique.

The semi-analytical finite element (SAFE) analysis was performed on an intact I-beam to investigate the dispersion characteristics and wave structure of each wave mode (Hayashi *et al*. 2003, 2006). The material parameters and cross-sectional dimensions of the steel I-beam are given in Table 1. Assuming that the beam is simply supported and bears the vertical downward cyclic loadings, fatigue cracks are prone to be initiated around the bottom weld zone between the web and lower flange. For the aim of crack detection, wave modes with high energy concentration in the bottom weld zone are preferred. Moreover, to localize the crack in the longitudinal axis of the beam, the number of the propagating wave modes shall be controlled as small as possible for the explicit interpretation of the time-history UGW signal.

Twenty-nine wave modes were found at 30 kHz from the previous SAFE analysis on the same structural member (Tu *et al*. 2021). Considering the multimode characteristics in the high-frequency range and the performance of the testing instrument, the central frequency of the excitation

Table 1 Material parameters and geometrical dimensions of I-beam

Young modulus (Gpa)	Poisson's Ratio	Density (kg/m^3)	Beam length (mm)	Thickness (mm)	Flange width (mm)	Web height (mm)	Sectional area of fillet weld (mm^2)
206	0.28	7850	1200	6	120	100	12.5

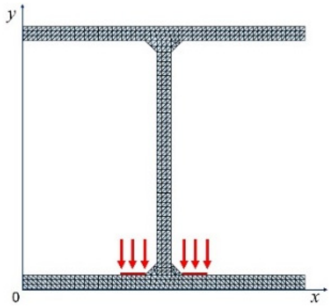

Fig. 1 SAFE model with vertical excitation

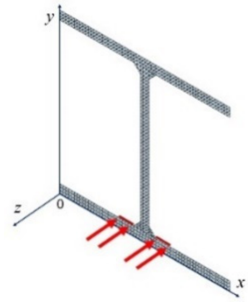

Fig. 4 SAFE model with horizontal excitation

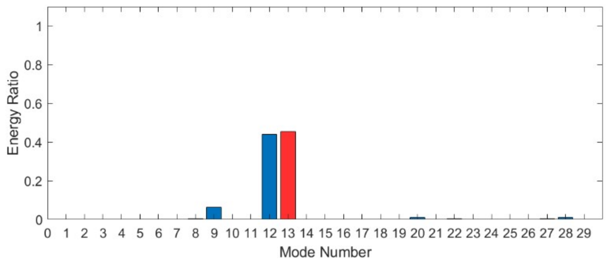

Fig. 2 Energy ratio of each wave mode at the bottom weld zone by applying vertical excitation at 30 kHz

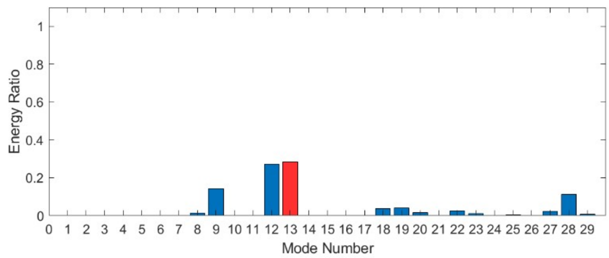

Fig. 5 Energy ratio of each wave mode at the bottom weld zone by applying horizontal excitation at 30 kHz

signal was preliminarily set in the range of 30-40 kHz with 2 kHz increments. By applying the vertical excitations near the weld zone as shown in Fig. 1, the dominant wave modes propagating in the welded intersection areas between the web and flanges are found to be Modes 12 and 13, as shown in Fig. 2. The wave structures of the two modes are plotted in Fig. 3. It shows that both Modes 12 and 13 have strong vibrations in three-dimensional directions, which guarantee the potential interaction between the propagating waves and the fatigue crack. At 30 kHz, the group velocities of Modes 12 and 13 by the SAFE analysis are 1626.5 m/s and 1591.6 m/s, respectively. For comparison, horizontal forces are also applied along the longitudinal axis, as illustrated in Fig. 4. The corresponding energy ratio of each wave mode at the bottom weld zone is shown in Fig. 5. It has been observed that the multi-mode effect, in this case, is more significant than that in the case of the vertical excitation. Some wave energy components shift to high-order wave modes, which generally has negative effects on the accuracy of crack detection. Very similar results have been observed with other excitation frequencies in 32-40 kHz.

2.2 Damage indices and signal processing

In this research, the conventional baseline subtraction residual method is adopted in the signal processing procedure for crack detection. The baseline is built upon the acquisition of UGW signals at the initial intact state. A set

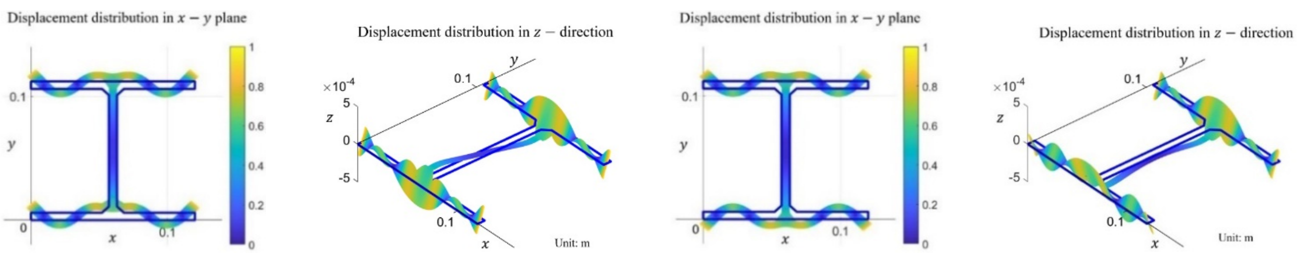

(a) Mode 12 (b) Mode 13

Fig. 3 Wave structures of Mode 12 and Mode 13 at 30 kHz of damage indices (DIs) is defined as follows.

- Relative cumulative residual squares: *RCRS* (Lu and Michaels 2005)

$$RCRS = \frac{\sum \tilde{a}^2}{\sum a^2} = \frac{\sum_{t=0}^{t=TIME}\left(a_{Base,t} - a_{Test,t}\right)^2}{\sum_{t=0}^{t=TIME}\left(a_{Base,t}\right)^2}, \tag{1}$$

where t is the time point; $a_{Base,t}$ is the baseline signal at t-th time point; $a_{Test,t}$ is the test signal at t-th time point; and $TIME$ is the total sampling time of the UGW signal.

- Segmental cross-correlation coefficient: *SCC* (Wang *et al.* 2020)

$$SCC(t) = \left|\frac{Cov\left(\boldsymbol{a}_{Base,t}, \boldsymbol{a}_{Test,t}\right)}{\sqrt{Var\left(\boldsymbol{a}_{Base,t}\right)Var\left(\boldsymbol{a}_{Test,t}\right)}}\right|, \tag{2}$$
$$\boldsymbol{a}_{Base,t} = [a_{Base,t} \quad a_{Base,t+1} \quad \cdots \quad a_{Base,t+\tau}],$$
$$\boldsymbol{a}_{Test,t} = [a_{Test,t} \quad a_{Test,t+1} \quad \cdots \quad a_{Test,t+\tau}],$$

where τ is the number of the sampling points of each segment. It is taken as the number of the sampling points of the excitation signal in this study.

- Acoustic nonlinear parameter: β' (Solodov *et al.* 2002, Lim and Sohn 2017)

$$\beta' = \frac{A^H}{(A^L)^2}, \tag{3}$$

where A^L and A^H are the maximum amplitudes of the fundamental guided waves and second harmonic waves in the frequency domain, respectively.

- Relative nonlinear parameter: β'_{re} (Lee *et al.* 2020)

$$\beta'_{re} = \frac{A^H}{A^L}, \tag{4}$$

The relative cumulative residual squares *RCRS* between the current test and baseline signals involves the amplitude changes and phase shifts of all the wave packets in the time domain. It is used to identify the existence of fatigue crack. The segmental cross-correlation coefficient *SCC* captures the amplitude and phase angle variations of each segment, which is used to estimate the crack location. The acoustic nonlinearity parameter β' is adopted to quantify the nonlinearity induced by local micro-cracks. It was derived based on the nonlinear Hook's law and the equation of wave propagation in isotropic plate-like structures (Fierro and Meo 2015). Another nonlinear parameter β'_{re} was derived based on a bi-linear stiffness model, which considered the change of elastic modulus under different pressure and tension. Compared with β'_{re}, β' amplifies the magnitude variation at the fundamental frequency. Both β' and β'_{re} have been used to detect the crack in the early state. The potential application of damage severity evaluation will be discussed by analyzing the variations of DIs through the experimental data.

The pulse-echo and pitch-catch methods are combined in the present detection strategy. In the pulse-echo mode, a pair of probes is placed at the left end of the beam for the signal excitation and echo acquisition as in Figs. 6 and 7. Signals obtained from this pulse-echo mode are filtered by the Morlet continuous wavelet transform (Rostami *et al.*

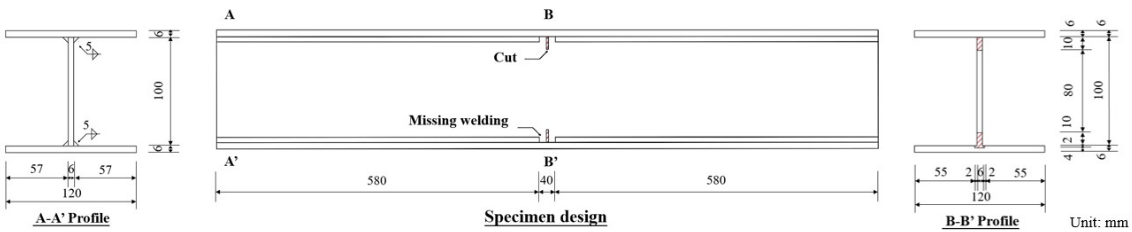

Fig. 6 Test specimen with initially inflicted damage

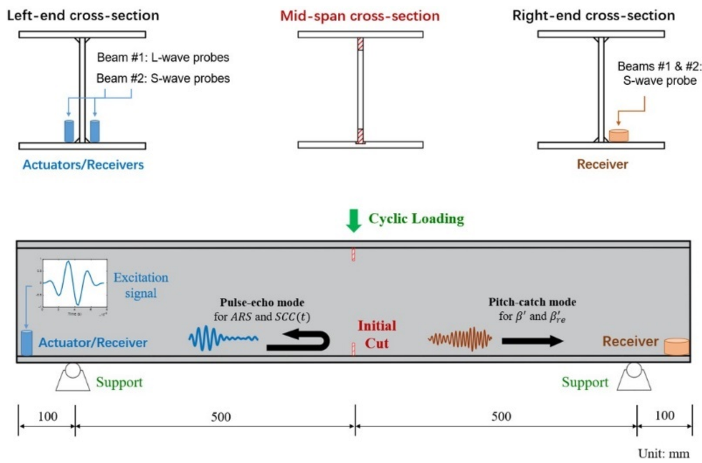

Fig. 7 Experimental setup

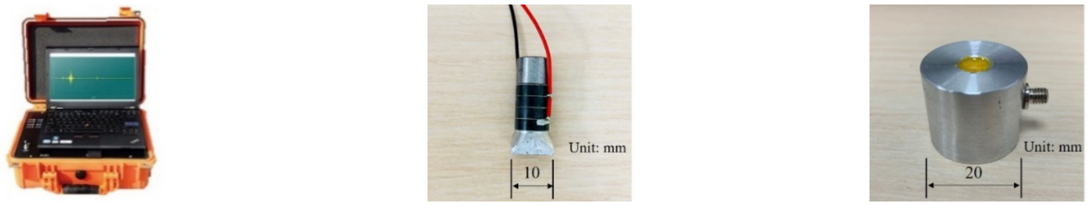

(a) UGWs detector (b) Longitudinal wave probe (c) Shear wave probe

Fig. 8 Equipment for UGW signal generation and acquisition

2017) to calculate the *RCRS* and *SCC* for crack identification and localization. In the pitch-catch mode, another single probe is placed at the other end of the beam to catch the transmitted waves. Signals from this probe are used to calculate the acoustic nonlinear parameters β' and relative nonlinear parameter β'_{re}. The Fast-Fourier Transform analysis is carried out on the raw signals to obtain the Fourier amplitude spectra (FAS) and the amplitudes of the fundamental and harmonic wave components (A^L and A^H).

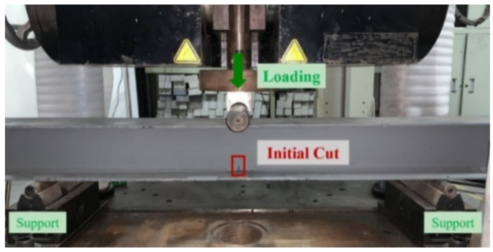

Fig. 9 Loading setup

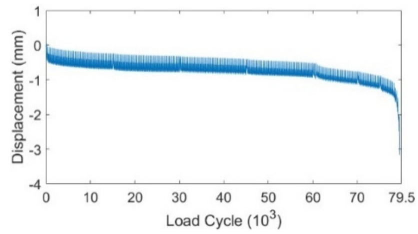

Fig. 10 Displacement curves of the loading point

3. Experiments

3.1 Experimental scheme

The specimen used in the experiments is shown in Fig. 6. The material parameters and cross-sectional dimensions have been shown in Table 1. The length of the steel I-beam is 1.2 m. The web plate and flange plates were connected by fillet welds. Before welding, two 1.0-cm-long cuts with a width of 4.0 mm and a depth of 6.0 mm were pre-machined on the upper and lower regions of the web plate at the mid-span of the beam (0.6 m from the left end). Another 1.0-cm-long cut with a width of 4.0 mm and a depth of 2.0 mm was inflicted in the middle of the bottom flange. The cuts were deliberately made to induce crack formations at the mid-span and accelerate the fatigue crack development process. For the same purpose, 4.0-cm-long regions on the upper and lower parts of the web at the mid-span were left without welding.

The experiment setup is illustrated in Figs. 7-9. Cyclic loads are applied at the mid-span in the three-point bending test mode to induce fatigue crack on the specimen as in Fig. 9. A pair of piezoelectric probes were bonded near the bottom weld zone at the left end of the beam by using Loctite EA E-05CL adhesive. The viscosity of the adhesive was 2500 Mpa·s, which guaranteed the firm adhesion of the bonding layer during the loading process. This pair of probes were connected in a parallel circuit to work as the actuators. Another piezoelectric probe was bonded at the right end of the beam, which worked as the receiver in the pitch-catch mode.

The equipment and probes used to generate and collect UGW signals are shown in Fig. 8. Two specimens of the same size were tested with two different types of excitation probes, to verify the results of wave propagation analysis from the SAFE model and determine an optimal excitation strategy. A pair of longitudinal wave (L-wave) probes were installed at the left end of Beam #1 for exciting and receiving as shown in Fig. 8(b). On the other hand, a pair of shear wave (S-wave) probes was installed at the left end of Beam #2 for exciting and receiving as shown in Fig. 8(c). The receivers at the right ends of Beams #1 and #2 were the same S-wave probe type. The UGWs detector developed by Hangzhou Zheda Jingyi Electromechanical Technology Corp (2015) was used for signal generation and acquisition. The sampling rate was set as 500 kHz, and the total time for the wave propagation was set as 0.02 seconds. The central frequency of the excitation signal was set in the range of 30-40 kHz with 2 kHz increments (six excitation frequencies in total). The excitation signal was selected as a sinusoidal wave modulated by a 3-cycle Hanning window in the pulse-echo mode. In pitch-catch mode, the excitation signal was reselected as a sinusoidal wave modulated by a 10-cycle Hanning window, to obtain significant changes in the fundamental waves and second harmonic waves for the receiver.

The loading setup is shown in Fig. 9. The Instron 8805 fatigue machine was used to apply loads in the three-point bending test mode. A sinusoidal cyclic force with a minimum of 8 kN and a maximum of 80 kN (stress ratio R = 0.1) was applied at the mid-span of the beam at a rate of 3 Hz. The loading process was paused every 5,000 cycles for the ultrasonic actuation and acquisition. For each excitation frequency, thirty UGW signals were collected at the initial

(a) Initial state (b) After 65,000 cycles (c) After 70,000 cycles

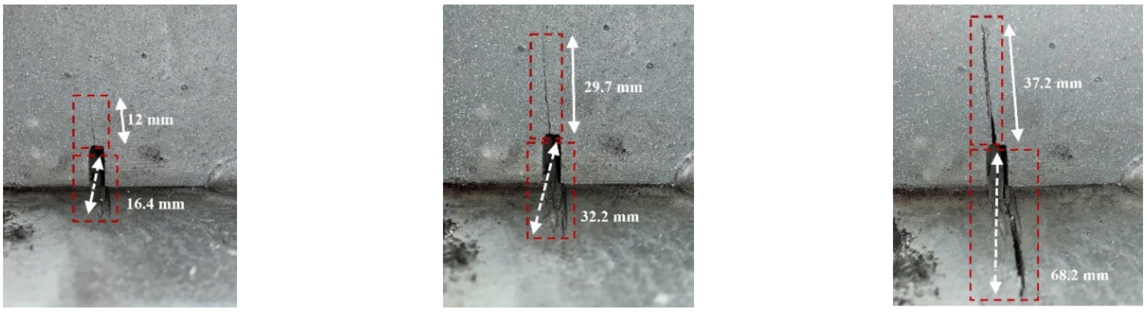

(d) After 75,000 cycles (e) After 77,500 cycles (f) After 79,500 cycles

Fig. 11 Fatigue crack development during cyclic loading test

state for baseline construction. And ten UGW signals were collected after each loading stage to determine the average of DIs. Each signal was an average of fifty excitation responses. The average is to reduce the possible noise interference. The test was stopped when the displacement of the loading point exceeded 1/400 of the total beam length, i.e., 3 mm in this research. The room temperature was controlled at around 22 degrees Celsius during the whole test process. By doing so, the influences of temperature variations on metallic material, wave probes, and wave propagations were minimized.

3.2 Experimental results

The experiment data presented in this section were obtained from Beam #1. The results from Beam #2 will be discussed in Section 5.2. For Beam #1, the downward displacement curve of the loading point obtained from Instron 8805 is shown in Fig. 10. It reflects the typical behavior of the metal fatigue fracture. As can be observed, the mean displacement increased slightly as the loading cycles increased, when the number of loading cycles was under 60,000. However, the displacement of the loading point begins to increase rapidly after about 78,000 cycles. After 79,500 cycles, the vertical position of the loading point exceeded by more than 3 mm, indicating the structural failure of the specimen. The loading test was stopped at this point.

The fatigue cracks growing at the intersection area of the mid-span are shown in Fig. 11. Visible crevices were observed on the bottom flange after 65,000 loading cycles. After 70,000 loading cycles, a crack about 8.6 mm long and less than 0.3 mm wide was developed from the cut inflicted on the web, and a crack about 13.2 mm long and less than 0.3 mm wide was also developed from the cut on the bottom flange. After 75,000 cycles of loading, the crack on the web further grew to about 12 mm long and 0.4 mm wide, and the crack on the bottom flange grew to about 16.4 mm long and 0.5 mm wide. Then, after 77,500 loading cycles, the cracks extended rapidly and reached the lengths of 29.7 mm and 32.2 mm on the web and flange, respectively, with a maximum width of about 0.6 mm. After 79,500 cycles, cracks with a maximum width of 1.9 mm were observed, and the specimen failed with an abrupt increase of the displacement at the mid-span.

Seventeen sets of the test UGW signals were collected after the loading began. The first 15 sets were collected after every 5,000 loading cycles until the loadings reached 75,000 cycles. The 16th set was collected after 77,500 loading cycles. And the final set was collected after the failure of the specimen at 79,500 cycles. Piezoelectric probes worked stably during the test. No visible deterioration was observed on the bonding layers during or after the test. Acetone solutions are required to remove the probes from the specimen for re-use.

The Morlet wavelet filter was used to process the raw signals. Fig. 12 shows a signal from L-wave actuators at the initial state of the specimen, which was filtered by the Wavelet transform of 30 kHz. The wave packet circled in the dashed line is the reflected wave packet from the right end of the beam. The propagating wave velocity of the dominant wave packet was obtained as 1726.9 m/s, based on the wave traveling distance (2.4 m) and the time interval between the Hilbert envelope peaks of the incident wave packet and reflected wave packet. The propagating velocity is found to be faster by 6.2% than the group velocity of Mode 12 in the SAFE model (1626.5 m/s). The geometric and material deviations of the specimen and the random

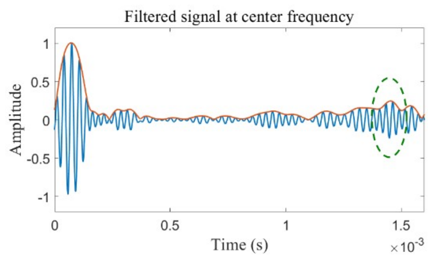

Fig. 12 Filtered signal from L-wave probe in pulse-echo mode at initial baseline state: Beam #1 at central excitation frequency of 30 kHz

vibrations of the bonding layer after excitation might cause the difference in the wave velocity between the experiment and the SAFE model (Tu *et al*. 2021, Zhang *et al*. 2018). The propagating velocity from the experiment is used to estimate the crack location in the following analysis.

UGW signals collected after several cases of loading cycles are shown in Fig. 13. The horizontal axis is converted into the acoustic distance of the UGWs based on the propagating velocity. It is observed that there are random phase and amplitude disturbances from 0.1 m to 0.35 m in the acoustic distance, due to the influence of electromagnetic oscillation and bonding layer vibration (Zhang *et al*. 2018) after excitation. This range is regarded as a detection blind zone and the associated wave information in this zone is neglected in the following analysis. With the increase of the loading cycles, the amplitude of the reflected waves from the crack location in the I-beam (at 0.6 m) gradually increases. And after 70,000 loading cycles, it began to rise significantly, while the amplitude of the reflected waves from the right end of the beam (at 1.2m) decreased significantly (Figs. 13(b) and (c)). The above changes in the amplitudes of the reflected waves can be observed more apparently in the residual signals subtracted from the baseline.

Fourier amplitude spectra of the signals from the S-wave probe at the right end of the beam in pitch-catch mode are shown in Fig. 14, along with the mean values from the baseline data for comparison. In the early loading stage, there is no significant difference in the FAS between the test and baseline cases (Fig. 14(a)). As the loading cycles increase, the peak amplitudes near the fundamental frequency (30 kHz) begin to shift and decrease, and the peaks near the double frequency (60 kHz) begin to rise (Figs. 14(b)). The variation trend of amplitude is enhanced by the increase of loading cycles. After 75,000 loading cycles, peaks at the second harmonic range reached the maximum (Fig. 14(c)). It is also observed that the amplitude variation in the second harmonic range is less noticeable than that in the fundamental frequency range. After 79,500 cycles, as the cracks at the mid-span grow wider than 1 mm, the magnitude of the second harmonic waves decreases (Fig. 14(d)).

4. Fatigue crack detection

Three DIs (*RCRS*, β', and β'_{re}) defined in Eqs. (1), (3), and (4) are used for the fatigue crack identification, and *SCC* defined in Eq. (2) is used for crack localization. Data from the experiment are processed to determine each DI. The threshold for crack warning (i.e., for *RCRS*, β', and β'_{re}) is set as the mean value plus three times the standard deviation (Jeon *et al*. 2019, Yang *et al*. 2019), which is determined based on baseline signals. When a crack warning is alarmed, the acoustic distance corresponding to the first local minimum of *SCC* is taken as the estimated crack location. To ensure the reliability of the estimated location d_{est}, the value of SCC_{dam} shall be less than 0.7, which means a statistically weak correlation between the baseline and test signals at the segment.

The variations of *RCRS* are shown in Fig. 15. It can be obtained that after 50,000 loading cycles, the *RCRS* exceeds the threshold and shows a trend of rising. It reaches the maximum after 77,500 loading cycles. At the end of the loading (after 79,500 cycles), the *RCRS* is 2.47 times the threshold. The variations of *SCC* for several other loading cycles are shown in Fig. 16. The time duration of each segment (τ as defined in Eq. (2)) is set to be equal to the

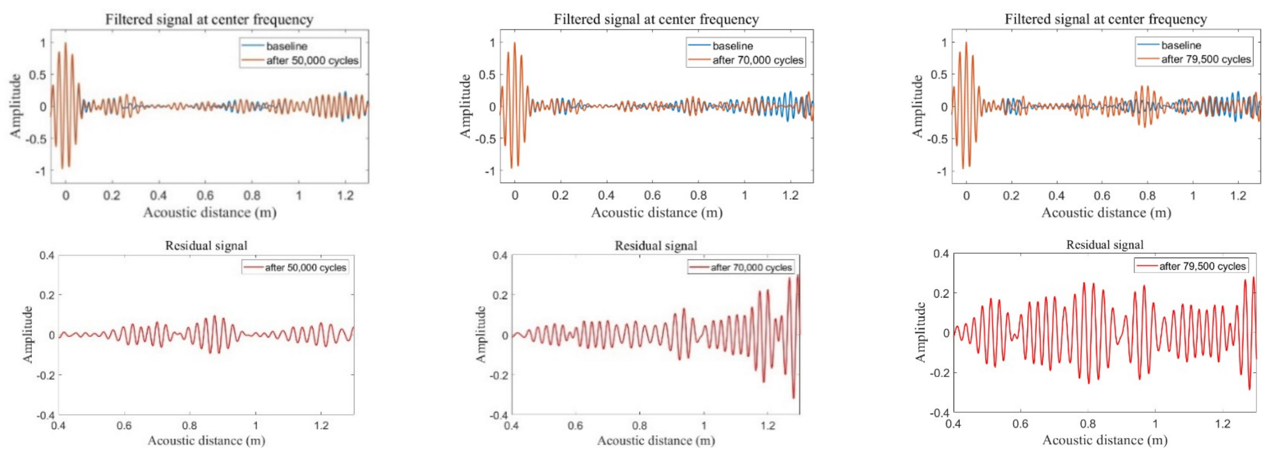

(a) After 50,000 cycles (b) After 70,000 cycles (c) After 79,500 cycles

Fig. 13 Filtered and residual signals from L-wave probe in pulse-echo mode after various loading cycles: Beam #1 at central excitation frequency of 30 kHz

(a) After 25,000 cycles

(b) After 50,000 cycles

(c) After 75,000 cycles

(d) After 79,500 cycles

Fig. 14 Fourier amplitude spectra from S-wave probe at the right end of Beam #1 in pitch-catch mode after various loading cycles: at central excitation frequency of 30 kHz

Table 2 Crack localizations by *SCC*: from L-wave probe in pulse-echo mode on Beam #1 at excitation frequency of 30 kHz

Loading cycles (10^3)	50	55	60	65	70	75	77.5	79.5
SCC_{dam}*	0.546	0.475	0.518	0.596	0.259	0.192	0.387	0.118
d_{est} (m)	0.634	0.62	0.608	0.595	0.615	0.608	0.611	0.411
$Error_{dam}$ (%)	2.82	1.67	0.66	0.42	1.23	0.66	0.94	15.75

*SCC_{dam}: the first local minimum of *SCC* in the acoustic distance of 0.35 m to 1.2 m;
$Error_{dam} = |(d_{est} - d_{true})/L|$, where d_{true} is 0.6 m and L is 1.2 m

length of the excitation wave packet. Taking the case of a 3-cycle Hanning window modulated signal at 30 kHz, the time duration of each analyzing segment is 0.0001s. At the early loading stage, no significant fluctuations of *SCC* are observed along with the acoustic distance (Fig. 16(a)). As the loading cycles increase, the *SCC* value near the mid-span of the beam (0.6 m) begins to drop (Fig. 16(b)). Several local minima appear between 0.6 m and 1.2 m of the beam (Fig. 16(c)). The predicted crack location by using the first local minimum is given in Table 2. After 50,000 cycles, the estimation error is found to be less than 2.82%, till the loading cycles reach 77,500. At the end of the loading, the first local minimum of *SCC* appears at a location (0.411 m) ahead of the mid-span (exact damage location), which leads to a larger localization error. It might be caused by the significant changes in the amplitude and phase of the wave packets at the final state as shown in Fig. 13(c).

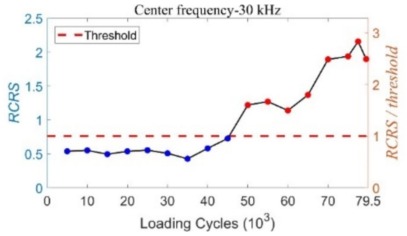

Fig. 15 *RCRS* versus loading cycles: from L-wave probe in pulse-echo mode on Beam #1 at central excitation frequency of 30 kHz

From the above discussions, it can be drawn that, when the baseline data at the initial intact state or a certain damage state are available, the UGWs approach by analyzing *RCRS* and *SCC* can issue an early warning and predict the crack location before the fatigue crack enters the rapid growth stage. As a rising trend is observed in the *RCRS* with increasing loading cycles, the severity of fatigue crack may be reasonably evaluated by monitoring the variations of *RCRS*.

UGW signals from S-wave probe is used to analyze the nonlinear DIs, which are related to the breathing crack that occurred on the bottom weld region of the I-beam. The variations of the acoustic nonlinear parameters, β' and β'_{re}, are shown in Fig. 17. For the case with a central excitation frequency of 30 kHz, A^L is taken as the maximum amplitude between 27 kHz and 33 kHz, and A^H is the maximum amplitude between 54 kHz and 66 kHz, considering the minor frequency shifts as observed in Fig. 14. The frequency range ($f \pm 3$ kHz for A^L, and $f \pm 6$ kHz for A^H) is identically applied to the other excitation frequency groups. The acoustic non-linear parameter β' slightly exceeds the threshold after 10,000 and 20,000 loading cycles, which may be caused by other uncertain factors such as noise interference. After 35,000 loading cycles, β' begins to be continuously higher than the threshold with fluctuations within a certain range. After 65,000 loading cycles, it begins to rise rapidly and reaches its peak at 75,000 loading cycles. Then it begins to fall and becomes lower than the threshold at the state of the structural failure. The relative nonlinear parameter β'_{re} remains below the threshold till 45,000 loading cycles. It exceeds the threshold after 50,000 loading cycles and begins to rise rapidly after 65,000 loading cycles. It reaches its peak after 75,000 loading cycles. Then it starts to fall and becomes below the threshold when approaching the failure of the specimen.

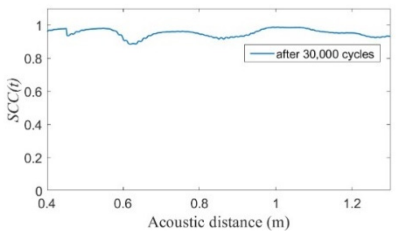

(a) After 30,000 cycles

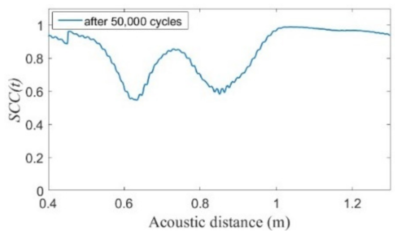

(b) After 50,000 cycles

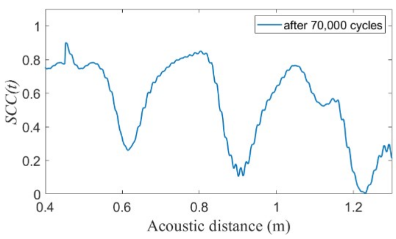

(c) After 70,000 cycles

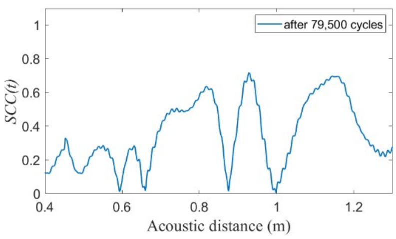

(d) After 79,500 cycles

Fig. 16 *SCC*(*t*) versus loading cycles: from L-wave probe in pulse-echo mode on Beam #1 at central excitation frequency of 30 kHz

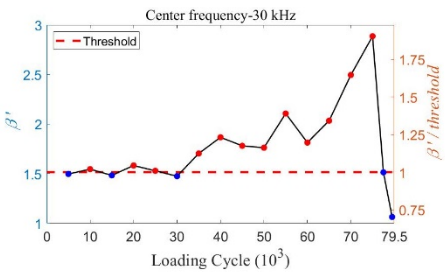

(a) β'

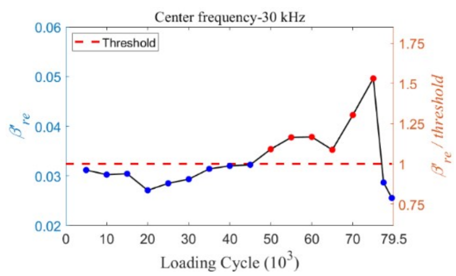

(b) β'_{re}

Fig. 17 Nonlinear damage indices versus loading cycles: from S-wave probe in pitch-catch mode on Beam #1 at central excitation frequency of 30 kHz

It is found that both *RCRS* and β'_{re} exceed the threshold after 50,000 loading cycles as shown in Figs. 15 and 17. It means that an early warning can be issued before the cracks become visible and grow rapidly. On the other hand, β' consistently exceeds the threshold after 35,000 loading cycles, which means that β' can issue an earlier warning. But there is also a possibility of false alarms due to noise interference (Yang *et al*. 2018, Lee *et al*. 2020). The combination of β', β'_{re}, and RCRS may provide a better evaluation of the damage severity. It is worth noting that there are a few other nonlinear methods, such as SPC-I technique (Alnuaimi *et al*. 2020, Basu *et al*. 2021), which have been shown to work better than linear techniques but have not been tried out in this study.

(a) 34 kHz (b) 40 kHz

Fig. 18 *RCRS* versus loading cycles: from L-wave probe in pulse-echo mode on Beam #1 at central excitation frequencies of 34 kHz and 40 kHz

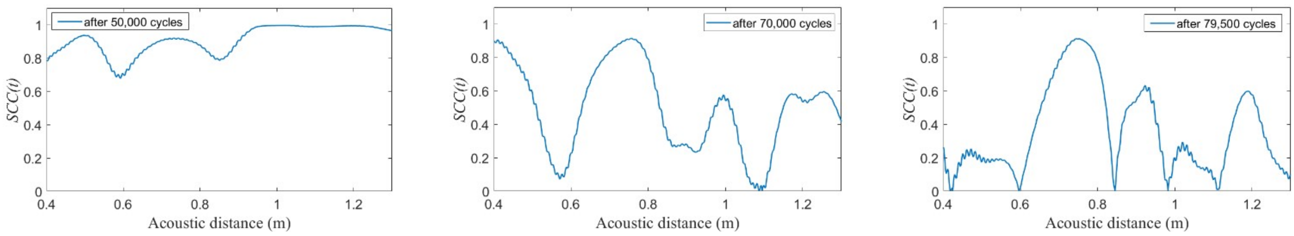

(a) 34 kHz

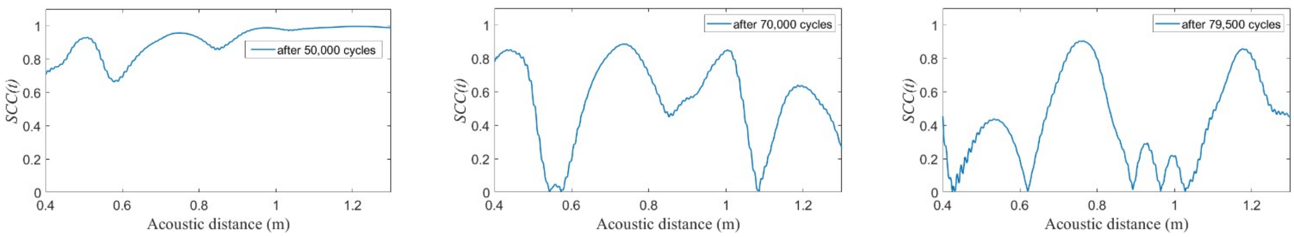

(b) 40 kHz

Fig. 19 *SCC*(t) versus loading cycles: from L-wave probe in pulse-echo mode on Beam #1 at central excitation frequencies of 34 kHz and 40 kHz

Table 3 Crack localization results by SCC: from L-wave probe on Beam #1 at excitation frequencies of 34 kHz and 40 kHz

	Loading cycles (10^3)	50	55	60	65	70	75	77.5	79.5
34 kHz	SCC_{dam}*	0.678	0.623	0.631	0.657	0.072	0.258	0.304	0.002
	d_{est} (m)	0.593	0.591	0.593	0.604	0.571	0.583	0.57	0.424
	$Error_{dam}$ (%)	0.583	0.750	0.583	0.333	2.416	1.417	2.50	14.667
40 kHz	SCC_{dam}	0.667	0.668	0.634	0.704	0.002	0.604	0.195	0.007
	d_{est} (m)	0.589	0.579	0.579	0.611	0.572	0.580	0.560	0.431
	$Error_{dam}$ (%)	0.917	1.750	1.750	0.942	2.333	1.667	3.333	14.083

*SCC_{dam}: the first local minimum of *SCC* in the acoustic distance of 0.35 m to 1.2 m;
$Error_{dam} = |(d_{est} - d_{true})/L|$, where d_{true} is 0.6 m and L is 1.2 m

(a) 34 kHz

(b) 40 kHz

Fig. 20 Nonlinear damage indices versus loading cycles: from S-wave probe in pitch-catch mode on Beam #1 at central excitation frequencies of 34 kHz and 40 kHz

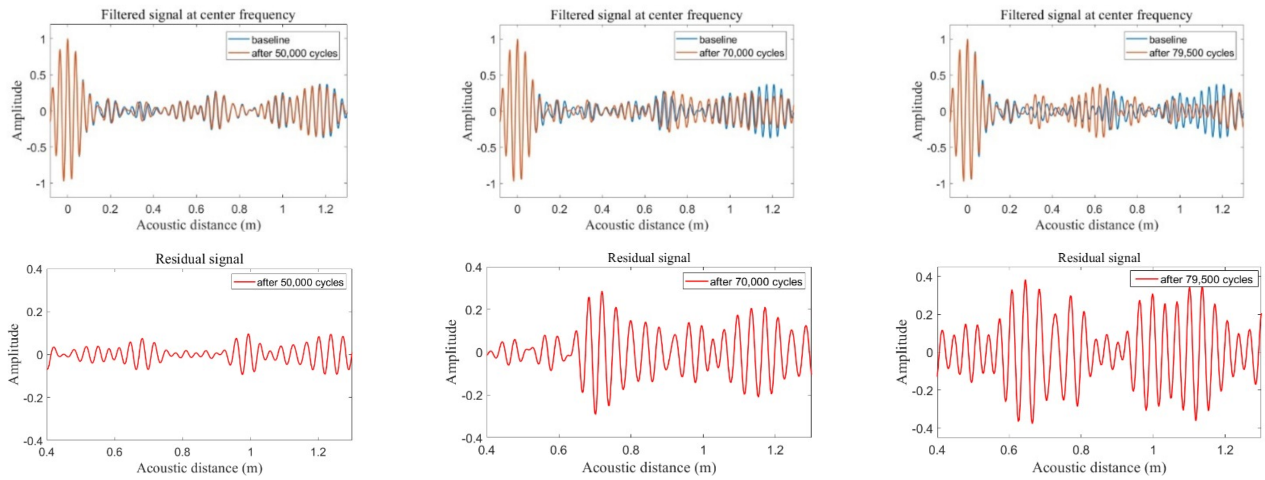

(a) After 50,000 cycles (b) After 70,000 cycles (c) After 79,500 cycles

Fig. 21 Filtered and residual signals from S-wave probe in pulse-echo mode: Beam #2 at central excitation frequency of 30 kHz

5. Factor analysis

5.1 Excitation frequency

In addition to 30 kHz, the UGWs-based crack detection is carried out at various excitation frequencies (32-40 kHz). Results for *RCRS* and *SCC* obtained at 34 and 40 kHz are plotted in Figs. 18 and 19. It can be observed that the *RCRS* starts to exceed the threshold after 50,000 loading cycles. It keeps rising and reaches its peak at 79,500 cycles. The results of crack localization by analyzing *SCC* are summarized in Table 3. After 50,000 loading cycles, the estimated crack location d_{est} corresponding to the first local minimum of SCC_{dam} begins to approach the exact crack location (0.6 m) as in Fig. 19. The localization error is found to be less than 3.4% at these two frequencies, excluding the last case of structural failure. It can be drawn that the results of crack identification and localization by analyzing *RCRS* and *SCC* are highly consistent and reliable.

UGW signals from the S-wave receiver under different excitation frequencies are processed to determine the nonlinear DIs. Results obtained at 34 and 40 kHz are plotted in Fig. 20. It can be seen that β' exceeds the threshold earlier than β'_{re} does during the loading process, which is identical to the result at 30 kHz. The nonlinear DIs from the signals at 34 kHz reach the maxima after 75,000 loading cycles, while those from the signals at 40 kHz reach the maxima after 70,000 loading cycles. Compared with *RCRS* and *SCC*, β' and β'_{re} are found to be more sensitive to the excitation frequency. When the crack width becomes greater than 1 mm, the nonlinear behavior of breathing cracks becomes weak. It is observed that β' and β'_{re} turn to decrease rapidly, even lower than the threshold. This result is consistent with that observed in the 30 kHz case.

5.2 Excitation probe

In Section 2.1, the wave energy distributions by two different excitation directions are compared based on the SAFE analysis. Another specimen, i.e., Beam #2, was tested under the same loading scheme but with the excitation by S-wave probes. It took 81,000 cycles for the structural failure of Beam #2. The baseline and seventeen sets of guided wave signals were collected at the initial and various loading stages as in Beam #1. Fig. 21 shows the UGW signals collected from the S-wave probes in pulse-echo

Table 4 Averages of crack localization results by SCC from L-wave probes and S-wave probes in pulse-echo mode after various loading cycles

Loading cycles (10^3)		50	55	60	65	70	75	77.5	79.5
L-wave probes (Beam #1)	$\overline{SCC_{dam}}^*$	0.638	0.601	0.604	0.648	0.082	0.351	0.297	0.060
	σ_{SCC}	0.049	0.066	0.046	0.049	0.104	0.155	0.069	0.059
	$\bar{d}_{est}$ (m)	0.598	0.590	0.588	0.601	0.581	0.587	0.570	0.423
	σ_d	0.020	0.017	0.013	0.006	0.020	0.012	0.025	0.014
	$\overline{Error_{dam}}$ (%)	0.201	0.824	0.964	0.042	1.567	1.057	2.468	14.764
S-wave probes (Beam #2)	$\overline{SCC_{dam}}$	-	-	-	0.597	0.25	0.413	0.587	0.546
	σ_{SCC}	-	-	-	0.145	0.301	0.235	0.121	0.106
	$\bar{d}_{est}$ (m)	-	-	-	0.574	0.516	0.509	0.563	0.553
	σ_d	-	-	-	0.118	0.065	0.068	0.113	0.110
	$\overline{Error_{dam}}$ (%)	-	-	-	2.147	7.042	7.569	3.069	3.889

*$\overline{SCC_{dam}}$: the average of SCC_{dam} from six excitation frequency groups; σ_{SCC}: the standard deviation of SCC_{dam};
$\bar{d}_{est}$: the average of crack localization results; σ_d: the standard deviation of $\bar{d}_{est}$;
$\overline{Error_{dam}}$: the average error of crack localization

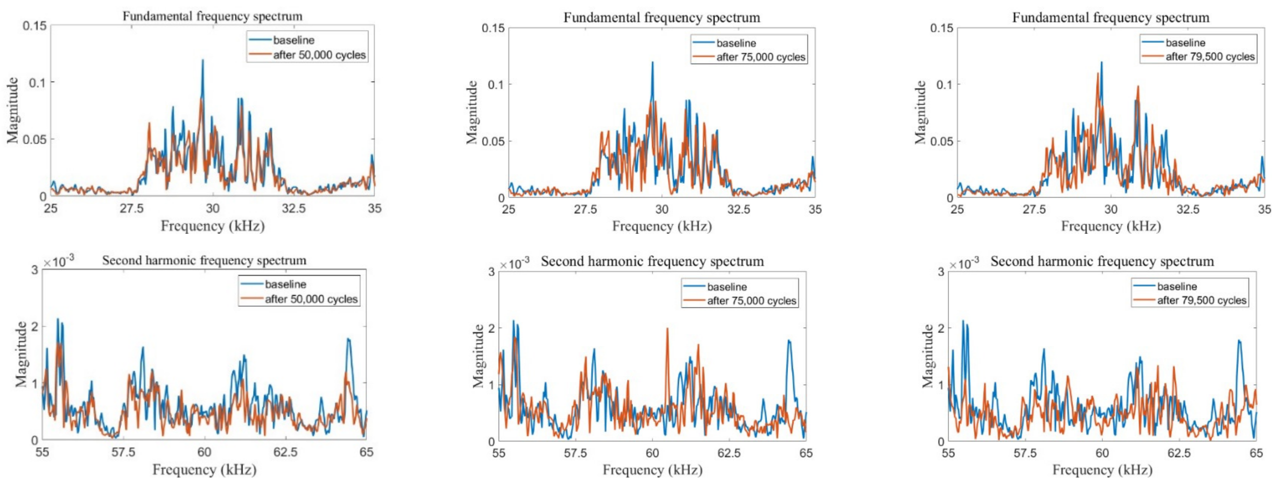

(a) After 50,000 cycles (b) After 70,000 cycles (c) After 79,500 cycles

Fig. 22 Fourier amplitude spectra from S-wave probe in pitch-catch mode: Beam #2 at central excitation frequency of 30 kHz

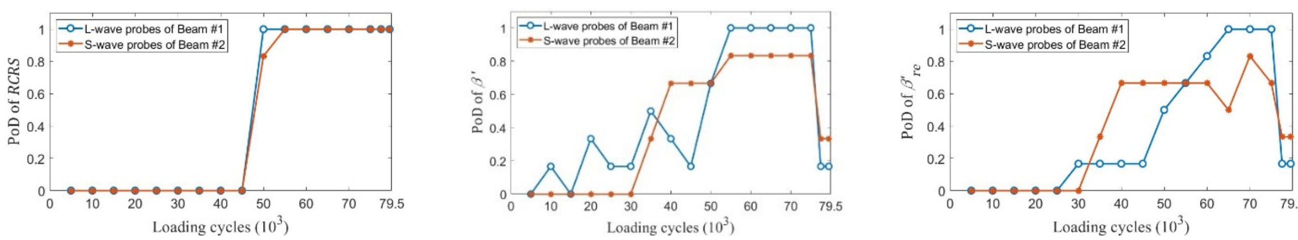

(a) $RCRS$ (b) β' (c) β'$_{re}$

Fig. 23 PoDs for Beam #1 and Beam #2

mode. As loading cycles increase, the amplitude of the wave packet from the crack at the mid-span gradually increases. After 70,000 loading cycles, the amplitude of the reflected waves from the right end drops significantly (Fig. 21(b)). Compared with the signals from the L-wave probe (Figs. 12 and 13), there are more scattered wave packets with higher amplitudes in the signals from the S-wave probe (Fig. 21). This observation indicates that although the S-wave probe input more energy in the normal direction to the plane of the major breathing crack, the propagation of guided waves under the excitation by the L-wave probe are found to be less affected by the dispersion effect. The FAS of the signals from the S-wave receiver are shown in Fig. 22. With the increase of loading cycles, the magnitude at the fundamental frequency range decreases, whereas the peaks of the second harmonic waves rise. After 75,000 loading cycles, the peaks of the second harmonic waves reach the maximum. Then, as the cracks grow wider, the magnitude of the second harmonic waves begins to drop.

Experiment data from six excitation frequency groups are compared between Beam #1 and Beam #2. An index 'probability of detection' (PoD) is defined as the ratio of the number of the frequency groups with DI exceeding the threshold to the total number of the excitation frequency groups (i.e., six: 30, 32, 34, 36, 38, and 40 kHz). The PoDs of *RCRS*, β', and β'_{re} are compared in Fig. 23. In the pre-selected excitation frequency range (30-40 kHz), it can be drawn that *RCRS* generally provides more reliable and consistent results for crack identification than β' and β'_{re} do. The *RCRS* can issue an early crack warning before the cracks grow rapidly. The nonlinear parameters β' and β'_{re} may issue crack warnings earlier, but they are more sensitive to the excitation frequency. The accuracy and reliability of the crack localization under the excitation of the L-wave probe are higher than those under the excitation of the S-wave probe as in Table 4.

6. Conclusions

In this study, experimental studies were carried out on the ultrasonic guided waves-based fatigue crack detection in a steel I-beam. Four damage indices were used for the detection and localization of the fatigue crack. To induce fatigue cracks on the beam specimens, sinusoidal loadings were applied at the mid-span in the three-point bending test mode. Longitudinal and shear wave probes were used in the pulse-echo and pitch-catch modes. Excitation frequencies of the ultrasonic guided waves (UGWs) were selected in the range of 30-40 kHz, considering the multi-mode characteristics and the performance of the experimental instrument. Conclusions are drawn as follows:

- The relative cumulative residual squares (*RCRS*) based on the time histories of the UGWs in the pulse-echo mode provided warnings for the fatigue crack existence after 50,000 loading cycles, when no visible crack was observed. The crack entered the rapid growth stage after 75,000 loading cycles and caused structural failure after 79,500 loading cycles.
- For the 1.2-meter-long I-beam, the segmental cross-correlation coefficients (*SCC*) based on the UGWs from the L-wave probes in the pulse-echo mode provided excellent crack localization results with an average error of less than 2.5%, after the existence of invisible crack was predicted. The performance of the *SCC* from the S-wave probes in the pulse-echo mode was less accurate with a maximum average error of 7.6%, though the S-wave probes initially input more energy perpendicular to the major fatigue crack surface.
- Two nonlinear damage indices, β' and β'_{re}, based on the amplitudes of the fundamental and second harmonic waves obtained in the pitch-catch mode gave earlier warnings of the fatigue crack at 35,000 and 50,000 loading cycles, respectively. Their performance was similar to that of the *RCRS*, after 55,000 and 65,000 cycles, respectively. For the nonlinear technique used in this study, the identification results are found be to less consistent under various excitation frequencies.

The work presented in paper is generally a proof-of-concept study. Further researches are suggested for the early fatigue crack detection using UGWs, including topics of the robustness to environmental effects, the fatigue damage severity evaluation, reference-free methods, and customized real-time systems for field applications.

Acknowledgments

The research described in this paper was financially supported by the National Key R&D Program of China (2021YFF0501002) and a research grant from the Center for Balance Architecture of Zhejiang University.

References

Alnuaimi, H., Amjad, U., Russo, P., Lopresto, V. and Kundu, T. (2020), "Monitoring damage in composite plates from crack initiation to macrocrack propagation combining linear and nonlinear ultrasonic techniques", *Struct. Health Monit.*, **20**(1), 139-150. https://doi.org/10.1177/1475921720922922

Basu, S., Thirumalaiselvi, A., Sasmal, S. and Kundu, T. (2021), "Nonlinear ultrasonics-based technique for monitoring damage progression in reinforced concrete structures", *Ultrasonics*, **115**, 106472. https://doi.org/10.1016/j.ultras.2021.106472

Bathias, C. and Pineau, A. (2013), *Fatigue of Materials and Structures: Fundamentals*, ISTE Ltd, London, UK.

Chua, C.A. and Cawley, P. (2020), "Crack growth monitoring using fundamental shear horizontal guided waves", *Struct. Health Monit.*, **19**(5), 1311-1322. https://doi.org/10.1177/1475921719882330

Dutta, D., Sohn, H., Harries, K.A. and Rizzo, P. (2008), "A Nonlinear Acoustic Technique for Crack Detection in Metallic Structures", *Proceedings of the Conference on Health Monitoring of Structural and Biological Systems*, San Diego, CA, USA, March.

Farrar, C.R. and Worden, K. (2009), "An introduction to structural health monitoring", *Proceedings of the Symposium on New Trends in Vibration Based Structural Health Monitoring*, Udine, Italy, September.

Fierro, G.P.M. and Meo, M. (2015), "Residual fatigue life estimation using a nonlinear ultrasound modulation method", *Smart Mater. Struct.*, **24**(2), 025040. https://doi.org/10.1088/0964-1726/24/2/025040

Garg, M., Sharma, S., Sharma, S. and Mehta, R. (2016), "Non-contact damage monitoring technique for FRP laminates using guided waves", *Smart Struct. Syst., Int. J.*, **17**(5), 795-817. https://doi.org/10.12989/sss.2016.17.5.795

Guan, S.Y., Rice, J.A., Li, C.Z., Li, Y.R. and Wang, G.C. (2015), "Dynamic and static structural displacement measurement using backscattering DC coupled radar", *Smart Struct. Syst., Int. J.*, **16**(3), 521-535. https://doi.org/10.12989/sss.2015.16.3.521

Hayashi, T., Song, W.J. and Rose, J.L. (2003), "Guided wave dispersion curves for a bar with an arbitrary cross-section, a rod and rail example", *Ultrasonics*, **41**(3), 175-183. https://doi.org/10.1016/S0041-624X(03)00097-0

Hayashi, T., Tamayama, C. and Murase, M. (2006), "Wave structure analysis of guided waves in a bar with an arbitrary cross-section", *Ultrasonics*, **44**(1), 17-24. https://doi.org/10.1016/j.ultras.2005.06.006

Hangzhou Zheda Jingyi Electromechanical Technology Inc. (2015), http://www.jingyitech.com

Hoła, J. and Schabowicz, K. (2010), "State-of-the-art non-destructive methods for diagnostic testing of building structures–anticipated development trends", *Arch. Civil Mech. Eng.*, **10**(3), 5-18. https://doi.org/10.1016/S1644-9665(12)60133-2

Jeon, I.G., Lim, H.J., Liu, P.P., Park, B.J., Heinze, A. and Sohn, H. (2019), "Fatigue crack detection in rotating steel shafts using noncontact ultrasonic modulation measurements", *Eng. Struct.*, **196**, 109293. https://doi.org/10.1016/j.engstruct.2019.109293

Kundu, T. ed. (2019), *Nonlinear Ultrasonic and Vibro-Acoustical Techniques for Nondestructive Evaluation*, Springer, Cham, Switzerland.

Lee, Y.F., Lu, Y. and Guan, R.Q. (2020), "Nonlinear guided waves for fatigue crack evaluation in steel joints with digital image correlation validation", *Smart Mater. Struct.*, **29**(3), 035031. https://doi.org/10.1088/1361-665X/ab6fe7

Lim, H.J. and Sohn, H. (2017), "Necessary conditions for nonlinear ultrasonic modulation generation given a localized fatigue crack in a plate-like structure", *Materials*, **10**(3), 248. https://doi.org/10.3390/ma10030248

Lim, H.J. and Sohn, H. (2020), "Online stress monitoring technique based on Lamb-wave measurements and a convolutional neural network under static and dynamic loadings", *Exp. Mech.*, **60**(2), 171-179. https://doi.org/10.1007/s11340-019-00546-8

Lim, H.J., Kim, Y., Sohn, H., Jeon, I. and Liu, P. (2017), "Reliability improvement of nonlinear ultrasonic modulation based fatigue crack detection using feature-level data fusion", *Smart Struct. Syst., Int. J.*, **20**(6), 683-696. https://doi.org/10.12989/sss.2017.20.6.683

Lu, Y.H. and Michaels, J.E. (2005), "A methodology for structural health monitoring with diffuse ultrasonic waves in the presence of temperature variations", *Ultrasonics*, **43**(9), 717-731. https://doi.org/10.1016/j.ultras.2005.05.001

Mariani, S. and Cawley, P. (2021), "Change detection using the generalized likelihood ratio method to improve the sensitivity of guided wave structural health monitoring systems", *Struct. Health Monit.*, **20**(6), 3201-3226. https://doi.org/10.1177/1475921720981831

Mitra, M. and Gopalakrishnan, S. (2016), "Guided wave based structural health monitoring: A review", *Smart Mater. Struct.*, **25**(5), 053001. https://doi.org/10.1088/0964-1726/25/5/053001

Molina, C.A. and Chapetti, M.D. (2018), "Estimation of high cycle fatigue behavior using a threshold curve concept", *Int. J. Fatigue*, **108**, 47-52. https://doi.org/10.1016/j.ijfatigue.2017.11.007

Niu, X.D., Marques, H.R. and Chen, H.P. (2018), "Sensitivity analysis of circumferential transducer array with T(0,1) mode of pipes", *Smart Struct. Syst., Int. J.*, **21**(6), 761-776. https://doi.org/10.12989/sss.2018.21.6.761

Olisa, S.C., Khan, M.A. and Starr, A. (2021), "Review of current guided wave ultrasonic testing (GWUT) limitations and future directions", *Sensors*, **21**(3), 811-838. https://doi.org/10.3390/s21030811

Raabe, D., Tasan, C.C. and Olivetti, E.A. (2019), "Strategies for improving the sustainability of structural metals", *Nature*, **575**(7781), 64-74. https://doi.org/10.1038/s41586-019-1702-5

Rehman, S.K.U., Ibrahim, Z., Memon, S.A. and Jameel, M. (2016), "Nondestructive test methods for concrete bridges: a review", *Constr. Build. Mater.*, **107**, 58-86. https://doi.org/10.1016/j.conbuildmat.2015.12.011

Rostami, J., Chen, J.M. and Tse, P.W. (2017), "A signal processing approach with a smooth empirical mode decomposition to reveal hidden trace of corrosion in highly contaminated guided wave signals for concrete-covered pipes", *Sensors*, **17**(2), 302. https://doi.org/10.3390/s17020302

Rykaluk, K., Marcinczak, K. and Rowinski, S. (2018), "Fatigue hazards in welded plate crane runway girders - Locations, causes and calculations", *Arch. Civil Mech. Eng.*, **18**(1), 69-82. https://doi.org/10.1016/j.acme.2017.05.003

Santecchia, E., Hamouda, A.M.S, Musharavati, F., Zalnezhad, E., Cabibbo, M., El Mehtedi, M. and Spigarelli, S. (2016), "A review on fatigue life prediction methods for metals", *Adv. Mater. Sci. Eng.*, **2016**, 9573524. https://doi.org/10.1155/2016/9573524

Schaal, C., Bischoff, S. and Gaul, L. (2016), "Damage detection in multi-wire cables using guided ultrasonic waves", *Struct. Health Monit.*, **15**(3), 279-288. https://doi.org/10.1177/1475921716642747

Solodov, I.Y., Krohn, N. and Busse, G. (2002), "CAN: an example of nonclassical acoustic nonlinearity in solids", *Ultrasonics*, **40**(1-8), 621-625. https://doi.org/10.1016/S0041-624X(02)00186-5

Tu, J.Q., Tang, Z.F., Yun, C.B., Wu, J.J. and Xu, X. (2021), "Guided wave-based damage assessment on welded steel I-beam under ambient temperature variations", *Struct. Control Health Monit.*, **28**(4), e2696. https://doi.org/10.1002/stc.2696

Wang, Z.J., Qiao, P.Z. and Shi, B.K. (2018), "Effective time-frequency characterization of Lamb wave dispersion in plate-like structures with non-reflecting boundaries", *Smart Struct. Syst., Int. J.*, **21**(2), 195-205. https://doi.org/10.12989/sss.2018.21.2.195

Wang, K., Cao, W.X., Su, Z.Q., Wang, P.X., Zhang, X.J., Chen, L.J., Guan, R.Q. and Lu, Y. (2020), "Structural health monitoring of high-speed railway tracks using diffuse ultrasonic wave-based condition contrast: theory and validation", *Smart Struct. Syst., Int. J.*, **26**(2), 227-239. https://doi.org/10.12989/sss.2020.26.2.227

Wu, J.J., Tang, Z.F., Lv, F.Z., Yang, K.J., Yun, C.B. and Duan, Y.F. (2018), "Ultrasonic guided wave-based switch rail monitoring using independent component analysis", *Meas. Sci. Technol.*, **29**(11), 115102. https://doi.org/10.1088/1361-6501/aadc47

Yang, Y., Ng, C., Kotousov, A., Sohn, H. and Lim, H.J. (2018), "Second harmonic generation at fatigue cracks by low-frequency Lamb waves: Experimental and numerical studies", *Mech. Syst. Signal Proc.*, **99**, 760-773. http://dx.doi.org/10.1016/j.ymssp.2017.07.011

Yang, S., Jung, J., Liu, P., Lim, H.J., Yi, Y., Sohn, H. and Bae, I.H. (2019), "Ultrasonic wireless sensor development for online fatigue crack detection and failure warning", *Struct. Eng. Mech.*, **69**(4), 407-416. https://doi.org/10.12989/sem.2019.69.4.407

Yu, X.D., Peng, Z., Jing, X. and Zheng, F. (2019), "Detection of damage in welded joints using high order feature guided ultrasonic waves", *Mech. Syst. Signal Proc.*, **126**, 176-192. https://doi.org/10.1016/j.ymssp.2019.02.026

Zhang, P.F., Tang, Z.F., Duan, Y.F., Yun, C.B. and Lv, F.Z. (2018), "Ultrasonic guided wave approach incorporating SAFE for detecting wire breakage in bridge cable", *Smart Struct. Syst., Int. J.*, **22**(4), 481-493. http://dx.doi.org/10.12989/sss.2018.22.4.481

Zhang, Y., Li, D.S. and Zheng, X.T. (2019), "Detection and location of bolt group looseness using ultrasonic guided wave", *Smart Struct. Syst., Int. J.*, **24**(3), 293-301. https://doi.org/10.12989/sss.2019.24.3.293

HJ